CrossMark

The Spectrum and Term Analysis of Singly Ionized Manganese

Florence S. Liggins[1] , Juliet C. Pickering[1] , Gillian Nave[2] , Jacob W. Ward[3,5] , and W.-Ü L. Tchang-Brillet[4]
[1] Physics Department, Imperial College London, Prince Consort Road, London SW7 2AZ, UK; j.pickering@imperial.ac.uk
[2] National Institute of Standards and Technology, Gaithersburg, MD 20899-8422, USA
[3] University of Maryland, College Park, MD 20742, USA
[4] Observatoire Paris-Site de Meudon, PSL University, Sorbonne Université, CNRS, LERMA, F-92190 Meudon, France
Received 2020 September 11; revised 2020 October 28; accepted 2020 November 1; published 2021 January 13

Abstract

An extensive analysis of the Mn spectrum was carried out using high-resolution Fourier transform (FT) and grating spectroscopy of Mn–Ne and Mn–Ar hollow cathode discharge sources, over the range 82–5500 nm ($1820–121{,}728\,\mathrm{cm}^{-1}$). Spectral wavelengths for a total of 6019 Mn II lines have been measured, of which 1345 are obtained through FT spectroscopy. These wavelengths are given to at least an order of magnitude lower uncertainty than previous measurements. These lines were used to identify 6256 Mn II transitions and improve the values of 505 previously published energy levels with typical uncertainties of a few thousandths of a cm^{-1}, representing an order-of-magnitude reduction in uncertainty. We have verified and improved an additional 57 Mn II energy levels, previously established through observation of stellar spectra alone, using our FT spectra. In addition, 52 new energy level values have been established. The number of classified lines reported is approximately 50% more than previously published. The new accurate data for 614 energy levels and 6019 lines will allow a more reliable analysis of Mn II spectral lines in astrophysical spectra.

1. Introduction

The range and resolution of spectra observed by advanced ground- and space-based telescopes and spectrographs (e.g., Hubble's Space Telescope Imaging Spectrograph, HST-STIS; the Very Large Telescope's Ultraviolet and Visual Echelle Spectrograph, VLT-UVES; and Keck II's High Resolution Echelle Spectrometer, HIRES, to name a few) have for decades been far exceeding those of the fundamental laboratory atomic data necessary for their analysis. There has been a concerted effort between Imperial College London (ICL), UK, and the National Institute of Standards and Technology (NIST), USA, to improve the atomic database of wavelengths and energy levels using high-resolution Fourier transform (FT) spectroscopy, with current focus on the neutral and singly ionized iron-group elements (Nave et al. 2017). Due to their complex atomic structure, the iron-group elements each contribute thousands of lines to the spectra of stars and other astrophysical plasmas, with transitions often contributing to blended profiles that require disentangling (Kurucz 2011).

The spectra of early-type stars, for example, are rich in lines due to transitions in the iron-group elements, largely of the first ionization stage. In particular, Mn II plays an important role in the study of late B-type, chemically peculiar, HgMn stars, for which there are observed abundance anomalies (Saffe et al. 2011). Their lines are typically sharp due to their characteristically low rotation velocities and weak magnetic fields. A discernible effort to understand the chemical make-up and evolution of these and other early-type stars (Schöller et al. 2013) has been fortified with new UV HST-STIS observations under the Advanced Spectral Library ASTRAL-II "hot stars" program (Carpenter & Ayres 2015).

The recent and projected analyses of these spectra rely heavily upon the accuracy and completeness of the atomic line database.

Modern stellar atmospheric models now consider three dimensions and take into account departures from local thermodynamic equilibrium (LTE). These elaborate 3D, non-LTE models are suitable for analyzing HgMn stellar atmospheres, for which there is an inferred inhomogeneity (Sigut 2001; Mashonkina 2010) and temporal variability (Makaganiuk et al. 2012) in the distribution of the atomic species. Among other parameters, however, such analysis requires a "complete set of atomic data on energy levels" for each given element (Mashonkina 2013).

This paper addresses the need for atomic data for Mn II and presents new and improved wavelengths and energy level values as a result of an extensive term analysis.

1.1. Previous Measurements of Mn II

The first extensive measurements of the manganese spectrum were carried out by Catalán (1923) using a Littrow spectrograph and concave grating instrument, over the range 230–400 nm. His identification of strong lines, grouped according to their similar characteristics, arguably led to the first use of the term "multiplet" and described transitions in Mn II, which were subsequently designated as $a\ ^7S - z\ ^7P°$, $a\ ^5S - z\ ^5P°$, $a\ ^5D - z\ ^5P°$, and $z\ ^7P° - e\ ^7D$.

Building on this, Curtis (1938) took grating measurements from the visible (620 nm) to the vacuum ultraviolet (VUV; 80 nm), from which 150 new levels of the septet and quintet term systems were found and 700 spectral lines classified. Use of the, then new, excitation mechanism of a hollow cathode lamp (HCL) allowed series to be observed relatively well and an ionization potential to be calculated.

---

[5] Associate, National Institute of Standards and Technology, Gaithersburg, MD 20899-8422, USA.

This study was then extended (Curtis 1952) by the classification of almost 600 additional lines, mostly due to transitions between triplet, or triplet and quintet, terms. From this, 101 new energy levels were established, of which many were triplets based on the $3d^6$, $3d^5(^4P)nl$, $3d^5(^4D)nl$, or $3d^5(^4G)nl$ subconfigurations. The system of quintets for the two lowest electronic configurations had been completed; however, the system of triplets was left incomplete, and no singlets had been identified.

Measurements made in the infrared wavelength region up to 990 nm by García-Riquelme et al. (1957) allowed the Mn II spectral analysis to be extended (Iglesias 1956, 1957); however, the disagreement between their measurements and Racah's calculations at the time (Racah & Shadmi 1959; Racah & Spector 1960) prompted a reanalysis by Iglesias & Velasco (1963), resulting in a revision of all low-lying septet, quintet, triplet, and singlet levels. Around 200 new levels were found with 500 Zeeman patterns, confirming the classifications.

The final summary of results from the analysis of the Mn II spectrum was then published as a monograph by Iglesias & Velasco (1964). It is predominantly these results which constitute the most recent compilation of Mn II (Kramida & Sansonetti 2013, hereafter KS), with wavenumber uncertainties ≈0.01–0.1 cm^{-1}. The compilation of KS also included around 100 Mn II wavelengths taken from more recent small-scale studies, enabling a reduction in uncertainty for around two thirds of the energy levels.

In addition, Joueizadeh et al. (1995) at the 5th International Colloquium on Atomic Spectra and Oscillator Strengths for Astrophysical and Laboratory Plasmas reported a preliminary analysis of Mn II based on a Fourier transform (FT) spectrum produced at Lund University using an iron hollow cathode coated in molten Mn. Their analysis, aided by the theoretical calculations of R. L. Kurucz (1994, private communication), led to the determination of 54 new energy levels of the $(^4G)4d$, $(^4P)4d$, $(^4D)4d$, and $(^6S)6d$ subconfigurations. The results of this unfinished analysis were never published, except for the wavelengths of one multiplet used for the identification of fluorescence lines in the red spectrum of η Carinae (Johansson et al. 1995). The list of the level energies was only available by private communication.

Since the compilation of KS, 73 new high-lying Mn II energy levels have been identified by Castelli et al. (2015, hereafter CKC) through HST-STIS and VLT-UVES spectral observations of the HgMn star HD 175640, the majority of which belong to the $3d^5(^4G)4d$, $3d^5(^4P)4d$, and $3d^5(^4D)4d$ configurations. Among these new energy levels, 25 were also in the unpublished list of Joueizadeh et al. (1995) and were in good agreement. The use of stellar spectra by CKC to find new energy levels in order to classify previously unidentified lines of Mn II attests to the urgency for new laboratory-measured atomic data for astrophysical analyses.

2. Experimental Details

Five sets of measurements were used in this analysis: (1) 17 FT spectra measured by Blackwell-Whitehead (Blackwell-Whitehead 2003; Blackwell-Whitehead et al. 2005) at ICL and NIST, for his work on neutral manganese; (2) one new FT spectrum measured at ICL for the purpose of Mn II analysis; (3) two FT spectra of a high-current HCL measured by Kling & Griesmann (2000) at NIST; (4) a set of 14 spectra using the

NIST normal incidence vacuum spectrograph (NIVS) using photographic plates and phosphor image plates; and (5) a set of 10 grating spectra recorded in 1994 at the Meudon Observatory. A summary of all spectra used in this analysis is given in Tables 1 and 2.

2.1. FT Spectroscopy

FT spectra used in this analysis are mostly taken from the measurements of Blackwell-Whitehead (2003), made over the range 1820–58,990 cm^{-1}. The region of 24,005–58,990 cm^{-1}, was recorded at ICL using both the IC ultraviolet (UV) FT spectrometer (Thorne et al. 1987) and IC VUV FT spectrometer (Thorne 1996). Infrared (IR) measurements were made at NIST over the region 1820–26,632 cm^{-1}, using the NIST 2 m FTS spectrometer. Since the measurements of Blackwell-Whitehead focused on Mn I, an additional high-current measurement of the region 33,897–58,990 cm^{-1} was made using the IC VUV FT spectrometer, optimizing the conditions of the source for Mn II.

Additional lines were taken from the high-current FT spectral measurements of Kling & Griesmann (2000). These measurements were recorded using the NIST FT700 UV FT spectrometer (Griesmann et al. 1999) for measurements of branching fractions. Although the strongest lines in these spectra are affected by self-absorption, the high current enabled some of the weaker transitions in Mn II to be observed.

The sources used were water-cooled HCLs run in either argon or neon. Due to the brittle nature of pure manganese, the cathodes for the 2001 spectra were made from a 95% Mn, 5% Cu alloy and those for the 1998 and 2012 spectra from an 88% Mn, 12% Ni alloy. These sources produce emission from Mn I and Mn II, the neutral and singly ionized spectra of the carrier gas used (Ar or Ne), and a number of metal lines from the alloy impurities. The HCL used by Blackwell-Whitehead at ICL was of a metal casing forming an anode, around an open-ended hollow cathode of 35 mm length and 8 mm bore (Blackwell-Whitehead 2003). The new ICL HCL consists of a 42 mm-long hollow cathode, placed at the center of a glass cylinder with grounded anodes at either end (Holmes 2015). The source used for all measurements made at NIST is a high-current, water-cooled HCL based on the design of Danzmann et al. (1988).

The spectral measurements of Blackwell-Whitehead were taken with gas pressures of 90 Pa of argon or 340 Pa of neon and a current of 450 mA. Lower current runs (200 mA) were also carried out for three spectra to account for self-absorption. The additional VUV spectrum made with the new IC HCL was measured with a higher current of 700 mA and neon gas pressure of 300 Pa. The resolution of these spectra ranged from 0.08 cm^{-1} in the VUV to 0.01 cm^{-1} in the IR. The measurements of Kling & Griesmann (2000) were made with the NIST HCL at a current of 2 A, pressure of 100–150 Pa of neon, and a resolution of 0.06–0.07 cm^{-1}.

The spectrum of a radiometrically calibrated standard lamp was recorded before and after each measurement of the manganese spectrum in order to determine the instrument response function at the time of measurement. This allowed relative line intensities to be obtained by dividing a given measured Mn spectral line intensity by the instrument response. A tungsten standard lamp was used for the visible to IR wavelength regions. The tungsten lamp used at ICL was calibrated by the National Physical Laboratory (NPL), UK. The

Table 1
FT Spectra Used in Mn II Analysis

Date/ Serial No.	Region Used (cm^{-1})	Instrument	Filter	Detector	Resolution (cm^{-1})	Current (A)	Pressure (Pa)	Gas Used	k_{eff}[a] /10^{-7}	Note[b]
2001 Jan 25 no. 2	1820–9550	NIST 2 m	⋯	InSb	0.01	1.2	75	Ar	2.50 ± 0.18	maah
2001 Jan 26 no. 3	1820–9550	NIST 2 m	⋯	InSb	0.01	1.5	250	Ne	1.31 ± 0.16	manh
2001 Jan 19 no. 4	4010–17,490	NIST 2 m	⋯	InSb	0.009	1.5	250	Ne	1.68 ± 0.07	mcnh
2001 Jan 22 no. 14	8520–24,985	NIST 2 m	⋯	Si	0.013	1.2	75	Ar	1.78 ± 0.03	meah
2001 Jan 16 no. 3	8443–25,291	NIST 2 m	⋯	Si	0.013	1.7	250	Ne	1.49 ± 0.06	menh
2001 Jan 16 no. 8	15,918–24,985	NIST 2 m	CuSO$_4$	Si	0.02	1.0	80	Ar	2.08 ± 0.02	mgah
2001 Jan 12 no. 16	15,993–26,632	NIST 2 m	CuSO$_4$	Si	0.02	2.0	250	Ne	3.41 ± 0.04	mgnh
2001 Mar 30	24,007–29,700	IC UV	Glass	1P28	0.04	0.45	90	Ar	2.26 ± 0.017	mjah
2001 Mar 27	24,057–29,786	IC UV	Glass	1P28	0.04	0.45	340	Ne	2.71 ± 0.05	mjnh
2001 Mar 27	24,779–27,567	IC UV	Glass	1P28	0.04	0.20	340	Ne	2.47 ± 0.06	mjnl
2001 Apr 2	25,421–41,943	IC UV	UG5	1P28	0.04	0.45	90	Ar	1.80 ± 0.06	mkah
2001 Mar 22	25,355–41,970	IC UV	UG5	1P28	0.04	0.45	340	Ne	2.41 ± 0.05	mknh
2001 Mar 26	35,690–35,770	IC UV	UG5	1P28	0.04	0.20	340	Ne	2.76 ± 0.07	mknl
2001 Apr 2	33,897–49,984	IC UV	⋯	R166	0.04	0.45	90	Ar	2.21 ± 0.12	mlah
2001 Mar 21 no. 2	33,897–52,425	IC UV	⋯	R166	0.04	0.45	340	Ne	2.21 ± 0.16	mlnh
2001 Mar 21 no. 1	35,770–35,806	IC UV	⋯	R166	0.04	0.45	340	Ne	2.26 ± 0.21	mlnl
2001 Dec 4	33,895–58,990	IC VUV	BP185	R1220	0.05	0.45	340	Ne	0.81 ± 0.29	mmnh
2012 Sep 13	33,897–58,990	IC VUV	BP185	R1220	0.08	0.70	300	Ne	13.30 ± 0.50	⋯
1998 Nov 12 no. 6	21,480–37,910	NIST FT700	⋯	R106UH	0.06	2.00	133	Ne	−1.32 ± 0.10	⋯
1998 Nov 12 no. 2	36,800–47,510	NIST FT700	⋯	R7154	0.07	2.00	150	Ne	8.76 ± 0.10	⋯

Notes.
[a] k_{eff}, the calibration correction factor for the spectrum with uncertainty.
[b] Name of spectrum as given in Blackwell-Whitehead (2003).

Table 2
Grating Spectra Used in Mn II Analysis

θ (°)[a]	Plate No.[b]	Region Used (nm)	Region Used (cm^{-1})	Filter	Note[c]
6.00	x1002#1	82.15–117.21	85,316–121,728	⋯	N0
7.00	x1002#1	117.22–146.15	68,422–85,309	MgF$_2$	N1
7.00	x1002#2	146.27–173.80	57,537–68,366	MgF$_2$	N2
9.00	x1002#1	173.80–203.96	49,029–57,537	MgF$_2$	N3
9.00	x1002#2	204.09–227.42	43,971–48,998	Silica	N4
11.00	x1002#1	227.43–254.25	39,331–43,969	Silica	N5
11.00	x1002#1	254.25–261.43	38,251–39,331	Silica	N6
11.00	x1002#2	261.70–294.50	33,955–38,211	Silica	N7
13.00	x1002#1	294.50–317.70	31,476–33,955	Silica	N8
13.00	x1002#2	318.80–352.30	28,385–31,367	Silica	N9
6.00	x976	83.2–114.3	120,192–87,489	⋯	⋯
7.00	x976	115.2–143.8	86,806–69,541	⋯	⋯
8.00	x976	143.8–171.7	69,541–58,241	⋯	⋯
9.00	x976	171.7–235.1	58,241–42,535	⋯	⋯
14.50	mn041194	108.0–121.3	92,593–82,440	⋯	⋯
15.50	mn041194	117.5–130.8	85,106–76,453	⋯	⋯
12.00	mn071194	84.5–97.8	118,343–102,249	⋯	⋯
13.25	mn071194	98.5–111.8	101,523–89,445	⋯	⋯
16.75	mn071194	129.2–142.5	77,399–70,175	⋯	⋯
18.00	mn071194	141.0–154.3	70,922–64,809	⋯	⋯
19.25	mn071194	152.7–166.0	65,488–60,241	⋯	⋯
20.50	mn081194	164.5–175.0	60,790–57,143	⋯	⋯
21.75	mn081194	176.0–188.5	56,818–53,050	⋯	⋯
23.00	mn081194	187.5–199.8	53,333–50,050	⋯	⋯

Notes.
[a] θ, angle of incidence.
[b] Plate #1 or #2 of measurement "x1002," taken at NIST on 2016 February 18–19. Plate x976 taken at NIST on 2013 July 18. Plates mn041194, mn071194, and mn081194 were taken at Meudon Observatory.
[c] Name of spectrum as given in Liggins (2017).

tungsten lamp used at NIST had a sapphire window for observations further into the IR and was calibrated by Optronics Laboratories, Inc.[6], FL, USA. Deuterium lamps were used with either fused silica or MgF$_2$ windows for our visible to UV and VUV spectra. These were calibrated at NPL, UK, and the Physikalisch-Technische Bundesansalt (PTB), Germany, respectively. Our spectra were placed on a consistent relative intensity scale by adjusting the scale of each spectrum so that strong lines in the overlapping regions of adjacent spectra had approximately the same value of relative intensity.

Relative level populations and the line intensities originating from these levels are dependent on the carrier gas, current, and pressure of the source. Since the list of observed spectral lines consists of measurements from several spectra obtained under varying conditions, the relative line intensities given here are only approximate, and we do not recommend them for the accurate determination of level branching fractions and transition probabilities.

The wavenumber, integrated intensity, FWHM, and signal-to-noise ratio (S/N) were obtained using the XGREMLIN software (Nave et al. 2015). Least-squares fits to Voigt profiles were carried out for lines with apparent symmetry. The centroid of the line profile was used for asymmetric lines and lines with significant hyperfine structure (HFS) broadening by taking a center-of-gravity (CoG) fit. This was the case for the majority of lines in our spectra.

A fit to the hyperfine pattern of a transition was sometimes necessary for particularly important lines where the wavenumber uncertainty was larger than expected from the S/N, such as

resonance transitions, key intercombination transitions, or lines where the transition identifications were deemed questionable. In these cases, fits to HFS were carried out using the routines of Pulliam (1979) that were incorporated into our XGREMLIN software. These routines iteratively fit the line using eight parameters: the HFS constants A and B for each level, the wavenumber, the FWHM, the Voigt damping parameter, and the S/N. Each parameter can be fixed to previously determined values and up to three transitions can be fitted to each spectral feature. HFS constants were taken from Townley-Smith et al. (2016) or Holt et al. (1999) where available. The fitting routines also derive the uncertainties of the parameters.

Wavelengths were calibrated using 26 Ar II standards (Learner & Thorne 1988) as recorded by Whaling et al. (1995) in the visible regime. Manganese lines taken from the calibrated Mn(Ar) visible spectra were then used to cross-calibrate Mn(Ne) spectra in the visible and spectra out into the IR and VUV regions. The uncertainty in wavenumber position due to calibration is cumulative with each successive spectrum in the cross-calibration procedure. It includes the uncertainty in the estimated calibration correction factor for the given spectrum and the uncertainty in the reference wavelengths used, going back to those of Whaling et al. (1995; ≈1 part in 10^8). The calibration factors and uncertainties for each spectrum are included in Table 1; further details of their uncertainty and cumulative uncertainty are given in Liggins (2017).

The total wavenumber uncertainty of a line in a single spectrum, δ_i, is given by the sum of the calibration uncertainty and the statistical uncertainty. Note that as the calibration uncertainty is common to all lines of a spectrum, it should be added directly to the statistical uncertainty and not in quadrature. The statistical uncertainty is derived from the fit of the spectral line $\delta\sigma_{\mathrm{fit}}$ using

$$\delta_{\mathrm{fit}} = \frac{\sqrt{(\mathrm{FWHM}) \times R}}{\mathrm{S/N}}, \tag{1}$$

as adapted from Equation (9.3) of Davis et al. (2001), where R is the resolution, in cm^{-1}, of the spectrum from which the line is taken. If the spectral lines were measured in several spectra, a weighted average, σ_{av}, of the measured wavenumbers, σ_i, was calculated, with the weights given by the reciprocal of the square of the total wavenumber uncertainty using

$$\sigma_{\mathrm{av}} = \frac{\sum_i \sigma_i \delta_i^{-2}}{\sum_i \delta_i^{-2}}. \tag{2}$$

The uncertainty of the wavenumbers was determined using

$$\Delta\sigma_{\mathrm{av}} = \sqrt{\frac{\sum_i (\sigma_i - \sigma_{\mathrm{av}})^2 \delta_i^{-2}}{(n-1)\sum_i \delta_i^{-2}}}, \tag{3}$$

where n is the number of measurements used in the wavenumber average. A minimum value of $1/\sqrt{\sum_i \delta_i^{-2}}$ was placed on the uncertainty in the weighted averaged wavenumber so that, should a small number of measurements happen to very closely coincide, the resulting uncertainty would not be unreasonably low. Including the calibration uncertainty of the individual spectra at this stage allows the appropriate weighting to be assigned to each measured line, depending not only on the quality of the line fit, but also the quality of the calibration of

the spectrum from which the line is taken. Finally, an uncertainty of 1×10^{-8} times the wavenumber or wavelength was added to all the uncertainties to account for the uncertainty of the original Ar II standard lines. In addition to the line wavenumbers, the total S/N of lines measured in multiple spectra was determined by adding the individual values in quadrature. The FWHM and integrated intensity of these lines was determined from the mean.

Since the calibration uncertainty changes throughout the wavenumber range and affects the uncertainty of the energy levels and Ritz wavelengths in a variable way, we adopted a minimum uncertainty of 5×10^{-8} times the wavenumber as a conservative estimate ($0.0005\,\mathrm{cm}^{-1}$ at $10,000\,\mathrm{cm}^{-1}$ or $1000\,\mathrm{nm}$; $0.0025\,\mathrm{cm}^{-1}$ at $50,000\,\mathrm{cm}^{-1}$ or $200\,\mathrm{nm}$). The value chosen corresponds to the maximum calibration uncertainty in Table 1 and also accounts for small discrepancies that we have observed in the calibration of the spectra when using different standard lines.

For cases where measurements of the HFS were made, the wavenumber position and uncertainty were determined from the least-squares fit of the HFS. This uncertainty was then added to the calibration uncertainty of the spectrum from which the line was taken. The wavenumber and other parameters previously obtained from the CoG fit to a given line were then replaced with those as given by the fit to HFS in our final line list.

A total of 15457 spectral lines were measured in our FT spectra. After multiple observations of the same line were averaged, the number of spectral lines in our final line list from these spectra was 9297. This number includes lines from all species present in the light source: Mn I, Mn II, as well as Ar, Ne, and impurities.

2.2. Grating Measurements

The Mn II spectrum was recorded in the region 28,385–121,728 cm^{-1} (352–82 nm) using the 10.7 m NIVS at NIST, USA. A 1200 line per millimeter, gold-coated grating blazed for 120 nm was used, giving a reciprocal dispersion in first order of 0.078 $\mathrm{nm\,mm}^{-1}$. Spectra were taken at angles of incidence from 6° to 13°. The slit width was 21 μm. Magnesium fluoride or fused silica filters were placed behind the entrance slit at angles of incidence from 6° to 13° in order to prevent second-order lines from shorter wavelengths from appearing in the region of interest. Details of the spectra are given in Table 2. The Mn II spectrum was produced by a high-current, water-cooled HCL (Danzmann et al. 1988), with a Mn/Ni foil placed inside a Cu hollow cathode. The lamp was run at a current of 2 A and at a pressure of 200 Pa neon as a carrier gas.

The Mn spectra were recorded onto Kodak[6] SWR photographic plates with an exposure time of 60 minutes. Spectra of a Pt–Ne HCL (Sansonetti et al. 1992) at angles of incidence 7° and 9° were recorded on tracks adjacent to the manganese spectra to give wavelength calibration standards. These measurements were carried out with a current of 20 mA and an exposure time of 2 hr. Photographic plates were used for the majority of the measurements due to their high sensitivity, wide wavelength coverage, and superior spatial resolution.

An additional 140 Mn II lines were taken from spectra recorded on Fuji BAS-TR 2040 image plates[6] (Nave et al. 2005) and scanned with a Perkin Elmer Cyclone[1] reader. The

same hollow cathode light source was used for these measurements, run at a current of 1.5 A and a pressure of 260 Pa of neon.

In addition to the grating spectra recorded at NIST, approximately 110 Mn II lines in our analysis were taken from grating spectra of a pulsed HCL recorded in 1994 using the 10.7 m normal incidence vacuum spectrograph at the Meudon Observatory. These spectrograms were originally recorded to complement the FT spectra from the University of Lund, Sweden (Joueizadeh et al. 1995). A 3600 line mm^{-1} grating was used, giving a linear dispersion of 0.025 nm mm^{-1} in first order, together with a 30 μm slit. The spectra were recorded on Kodak[6] SWR photographic plates in the range 84.5–199.8 nm. The light source was a copy of the hollow cathode source developed in Lund but equipped with a pure solid manganese cathode cut out by electro-erosion and inserted into a brass holder. The source was operated in a pulsed mode with 70–90 Pa of Ne as carrier gas. The discharges were produced with a peak current of 180–250 mA, using a 10 μF capacitor charged between 700 and 900 V. In this operating mode, the spectrograms produced a very complete Mn II spectrum and at the same time the strongest multiplets of Mn III (Tchang-Brillet & Azarov 2002).

The positions of the spectral lines on both the NIST and Meudon photographic plates were measured using a Grant Instruments[6] spectrum plate comparator, based on the design of Tomkins & Fred (1951) with an added digital encoder. A visual estimate of the intensity of each line was also recorded.

Wavelength calibration of the NIST plates was carried out using Pt standard lines (Sansonetti et al. 1992) in the region 117–254 nm. Below 117 nm, where no Pt–Ne tracks were recorded, it was possible to exploit the use of the Cu cathode, by calibrating using Cu II Ritz wavelengths derived from Kramida et al. (2017). Mn II wavelengths from the calibrated FT spectra, as described in Section 2.1, were then taken for calibration of the remaining spectral regions. These standard lines were used to estimate the dispersion of the grating spectra by fitting polynomials of orders between 6 and 10 using around 30–100 lines for each track, evenly spaced throughout the measured spectral range. Further details can be found in Liggins (2017). The standard deviation of the wavelength calibration varied from 0.08 pm to 0.2 pm.

Wavelengths from the Meudon spectrograms were calibrated using internal standards provided either by previous Mn II Ritz wavelengths from Joueizadeh et al. (1995) or by wavelengths of impurity lines. The calibration agrees with that of the NIST plates to within 0.5 pm.

The total wavelength uncertainty for a given line in our grating spectra was estimated according to the strength and quality of the line. For lines assigned an intensity greater than 5 and less than 60 (i.e., strong enough to measure an accurate position but not saturated), and where the line had no associated qualifier on the intensity (hazy, broadened, etc.), the total wavelength uncertainty was estimated to be approximately 0.0002 nm (0.05 cm^{-1} at 50,000 cm^{-1}). The uncertainty of the remaining lines was estimated to be 0.0005 nm. The intensities given for grating measurements in Table 3 are visual estimates of the plate density, and they should therefore be seen only as an approximate guide to the relative strengths of the lines. The line list from our grating spectra contained about 13,957 lines, of which 12,371 lines in the wavelength region 82–352 nm were measured in the NIST spectra using

photographic plates, 753 lines from 88 to 235 nm in the NIST spectra using phosphor image plates, and 833 lines from 86 to 200 nm in the Meudon spectra of a pulsed hollow cathode.

3. Mn II Spectral Analysis

3.1. Line Identification

The initial identification of Mn II lines in the line list was carried out using the compiled energy level values of KS, the majority of which are taken from the monograph of Iglesias & Velasco (1964). In addition, new levels that had been identified by CKC were used to identify possible Mn II transitions in our FT spectra. Lines due to Mn I transitions were identified using the updated energy level values of Blackwell-Whitehead (2003). Ar I and Ar II were identified using the measurements of Whaling et al. (2002, 1995), and for Ne I and Ne II, the measurements of Saloman & Sansonetti (2004) and Kramida & Nave (2006) were used, respectively. Impurity lines from Ni I were identified using the line list of Litzén et al. (1993) and lines of Ni II using the line list of C. Clear at Imperial College (Clear 2018). Lines of Cu I were taken from the NIST Atomic Spectra Database (Kramida et al. 2019) and those of Cu II were taken from Kramida et al. (2017). Lines of Ni II and Cu II were very weak on our photographic plates above 120 nm as spectra from these ions are poorly excited by a pure neon carrier gas in this wavelength region. However, spectral lines of Cu II below 120 nm are from low energy levels that are excited in pure neon.

Accurate wavenumbers for blended lines could sometimes be derived by fitting the HFS, using previously measured HFS constants for one or both transitions where available. Figure 1 gives an example of where FT spectroscopy has enabled a blend of two transitions to be resolved, one of which is the hyperfine-split $z^5P_3^o - b^5D_4$ transition in Mn II. The line wavenumber taken from previous measurements would have been affected by that of the contributing unidentified transition (blue), and the entire profile, described by Iglesias & Velasco (1964) as "extremely hazy," would have been unresolved.

3.2. The Mn II Spectrum

During this analysis, a total of 6019 observed lines have been classified with 6256 transitions in singly ionized manganese. Of these, 1345 lines classified with 1364 transitions (some lines being multiply identified) were measured using high-resolution FT spectroscopy. All observed Mn II transitions are presented in Table 3.

The first column gives the method of measurement of the line with the key to the method given in the footnote of the table. The intensity in the second column is an integrated relative intensity. For our FT spectra, labeled "F" or "h" in column 1, the intensities were calibrated using standard lamp spectra as described in Section 2.1. Since the source conditions vary from spectrum to spectrum, the intensities should be regarded as approximate values and are not recommended for determining branching fractions or oscillator strengths. Line intensities in our grating spectra measured on photographic plates, labeled "g" or "P" in column 1, are visual estimates of the plate blackening and are on a different scale than our FT spectra. An additional qualifier to the intensity denotes if the line appeared wide, asymmetric, or hazy, as given in the table footnote. Lines that were measured on image plates, labeled "I"

Table 3
Observed Lines of Mn II

Origin	Int.	FWHM (10⁻³ cm⁻¹)	S/N	λ_{air} (nm)	λ_{vac} (nm)	Unc. (nm)	σ_{obs} (cm⁻¹)	Unc. (cm⁻¹)	λ_{Ritz} (nm)	Unc. (nm)
(1)	(2)	(3)	(4)	(5)	(6)	(7)	(8)	(9)	(10)	(11)
F	182	123	19	283.07189	283.15516	0.00006	35,316.326	0.008	283.15516	0.00006
F	45	154	4	283.0465	283.1298	0.0003	35,319.49	0.04	283.13002	0.00007
A	2			283.0158	283.0990	0.0015	35,323.33	0.19	283.09904	0.00003
g	25 l			282.9338	283.0170	0.0005	35,333.57	0.06	283.01666	0.00008
g	40			282.89697	282.98020	0.00020	35,338.161	0.025	282.98029	0.00003
g	40			282.89697	282.98020	0.00020	35,338.161	0.025	282.97987	0.00011
g	60			282.88397	282.96720	0.00020	35,339.785	0.025	282.96704	0.00005
g	10			282.86477	282.94800	0.00020	35,342.183	0.025	282.94774	0.00009
g	45			282.84678	282.93000	0.00020	35,344.431	0.025	282.93001	0.00010
g	45			282.84678	282.93000	0.00020	35,344.431	0.025	282.93010	0.00010
g	40			282.83808	282.92130	0.00020	35,345.518	0.025	282.92129	0.00004
g	55			282.62793	282.71110	0.00020	35,371.80	0.03	282.71114	0.00006
g	10 p			282.5228	282.6059	0.0005	35,384.96	0.06	282.60645	0.00003
g	30 p			282.5189	282.6020	0.0005	35,385.45	0.06	282.60181	0.00010
g	55 l			282.5143	282.5974	0.0005	35,386.03	0.06	282.59716	0.00004
F	176	399	7	282.4680	282.5511	0.0003	35,391.83	0.04	282.55123	0.00008
F	47	287	9	282.40167	282.48478	0.00019	35,400.137	0.024	282.48467	0.00005

| Transition						E_L (cm⁻¹)	E_U (cm⁻¹)	Notes
Lower level			Upper level					
(12)			(13)			(14)	(15)	(16)
$3d^5(^2H)4s$	$a\ ^1H$	5	$3d^5(^2H)4p$	$y\ ^1I°$	6	51,553.094	86,869.420	
$3d^5(^2D)4s$	$c\ ^3D$	1	$3d^5(a^2D)4p$	$x\ ^3F°$	2	44,139.039	79,458.501	
$3d^6$	$a\ ^3H$	6	$3d^5(^4G)4p$	$z\ ^5H°$	7	30,523.685	65,847.0114	
$3d^5(^2D)4s$	$b\ ^1D$	2	$3d^5(^4F)4p$	$x\ ^5F°$	1	46,903.328	82,236.937	
$3d^6$	$b\ ^3G$	3	$3d^5(^4D)4p$	$y\ ^5F°$	3	35,004.805	70,342.9555	II #
$3d^5(^2F)4s$	$d\ ^3F$	2	$3d^5(a^2G)4p$	$u\ ^3F°$	3	52,379.468	87,717.670	II #
$3d^5(^4P)4p$	$y\ ^5P°$	1	$3d^5(^4P)5s$	$e\ ^5P$	2	68,496.6985	103,836.503	
$3d^5(^2G)4s$	$b\ ^1G$	4	$3d^5(^2H)4p$	$w\ ^3H°$	5	52,653.357	87,995.572	
$3d^6$	$e\ ^3F$	3	$3d^5(a^2G)4p$	$^3G°$	3	52,373.239	87,717.670	II #
$3d^5(^2F)4s$	$d\ ^3F$	3	$3d^5(a^2G)4p$	$u\ ^3F°$	3	53,781.735	89,126.154	II #
$3d^5(^4D)4p$	$y\ ^5D°$	3	$3d^5(^4G)4d$	^5D	2	72,247.7621	107,593.282	
$3d^5(^4P)4p$	$y\ ^5P°$	1	$3d^5(^4P)5s$	$e\ ^5P$	1	68,496.6985	103,868.492	
$3d^5(^4P)4p$	$z\ ^5D°$	4	$3d^5(^4G)5s$	$e\ ^3G$	5	67,295.4490	102,680.346	
$3d^5(^4D)4p$	$y\ ^3P°$	1	$3d^5(^4P)4d$	^3P	0	75,719.981	111,105.459	
$3d^5(^4P)4p$	$y\ ^5P°$	2	$3d^5(^4P)5s$	$e\ ^5P$	3	68,417.7040	103,803.764	
$3d^5(^2F)4s$	$b\ ^3F$	4	$3d^5(a^2D)4p$	$x\ ^3F°$	4	44,521.540	79,913.352	
$3d^5(^2D)4s$	$b\ ^1D$	2	$3d^4(^5D)4s4p(^3P)$	$^7F°$	3	46,903.328	82,303.479	

Note. The columns are as follows: (1) the origin of the line: F—line measured in FT spectra; h—line measured in FT spectra with wavenumber determined by fitting the HFS; G—line measured in grating spectra of a continuous hollow cathode on photographic plates; P—line measured in grating spectra of a pulsed hollow cathode on photographic plates; I—line measured in grating spectra of a continuous hollow cathode on image plates; A—line taken from the NIST Atomic Spectra Database (Kramida et al. 2019). (2) The relative intensity of the line. The intensities from the FT and grating spectra are on different scales. Lines measured on photographic plates are visual estimates of the plate blackening, with the qualifiers: w—wide, b—broad, s—shaded to short wavelengths, l—shaded to long wavelengths, p—perturbed (e.g., on a wing of a stronger line), h—hazy, q—position questionable, c—complex (central position is blend of 3 or more lines). (3) The FWHM of the line in units of 0.001 cm⁻¹. (4) The signal-to-noise ratio of the line. (5) λ_{air}: the observed air wavelength, in nanometers, given between 200 and 2000 nm. (6) λ_{vac}: The observed vacuum wavelength, in nanometers. (7) The uncertainty in the air and vacuum wavelengths. (8) σ_{obs}: the observed vacuum wavenumber of the transition, in cm⁻¹. (9) The uncertainty in σ_{obs}, in cm⁻¹. (10) λ_{Ritz}: the Ritz vacuum wavelength in nanometers derived from the optimization of the energy levels. (11) The uncertainty in the Ritz wavelength. (12) The configuration, term, and J value of the lower level. (13) The configuration, term, and J value of the upper level. (14) E_L: the lower energy level value in cm⁻¹. (15) E_U: the upper energy level value in cm⁻¹. (16) Notes: Multiply classified with Mn I, Mn II, or Mn III ("I", "II", "III"), or another element. Lines marked with a # were given a low weight in the energy level optimization.

(This table is available in its entirety in machine-readable form.)

in column 1, were determined using a Gaussian fit to the line profile and are on a different scale than the other intensities.

A guide to the width of the line profile is given in column 3, in units of 0.001 cm⁻¹, and in column 4, the S/N is provided. The observed air wavelength in column 5 is given in the region between 200 nm and 2 μm, and is determined in standard air using the five-parameter dispersion formula of Peck & Reeder (1972). The vacuum wavelength in nanometers and the observed vacuum wavenumber in cm⁻¹ from which these are determined are given in columns 6 and 8, respectively. The results have been rounded so that the uncertainty in units of the last digit does not exceed 25. The one standard
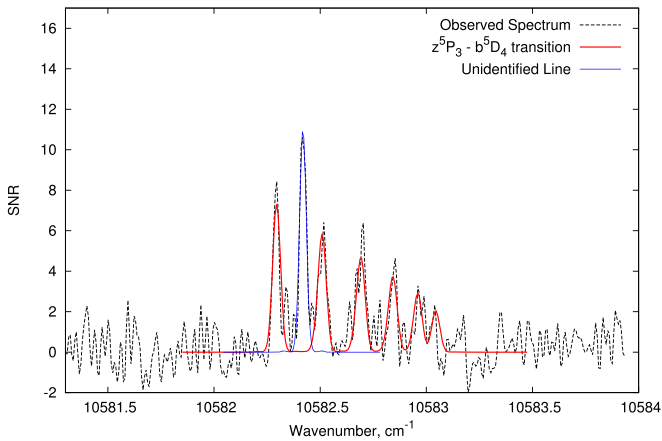
Figure 1. The hyperfine-split profile of the $z^5P_3^\circ - b^5D_4$ transition as observed (black) and fitted (red). FT spectroscopy resolves this as a blend with an unidentified transition (blue).

uncertainties in the observed wavelengths and wavenumbers are given in column 7 and 9, respectively. The calculated Ritz wavelengths and one standard uncertainties are provided in columns 10 and 11. Ritz wavelengths are given in air between 200 nm and 2 μm and in vacuum elsewhere. The transition classifications, giving the labels for the designated lower and upper levels, are shown in columns 12 and 13, with the energy level values in cm^{-1} given in columns 14 and 15. The final column marks any blends and lines that were given a low weight in the energy level optimization.

The wavenumber uncertainties of strong lines in our FT spectra are typically an order of magnitude lower than those of previous measurements (Iglesias & Velasco 1964) and range from ≈ 0.001 to $0.01\ cm^{-1}$. Lines in our grating spectra that are neither saturated nor blended have uncertainties of 0.0002 nm ($0.05\ cm^{-1}$ at $50,000\ cm^{-1}$).

4. Atomic Structure of Mn II

Manganese is a transition element belonging to the ($3d$) iron group of elements, with the ground level $3d^54s\ a\ ^7S_3$. The nd and $(n + 1)s$ electrons of these elements are known to have very similar binding energies. There is thus some overlap in the three lowest configurations of Mn II, $3d^6$, $3d^54s$, and $3d^44s^2$, and so it is possible to observe apparent two-electron transitions due to configuration interaction. Within a single configuration, several different LS components may contribute a substantial fraction to each energy level, allowing many ordinarily LS-forbidden intercombination transitions to occur.

A schematic diagram of the terms in Mn II can be seen in Figure 2. The excited electronic configurations of Mn II are split into the singly excited (normal) and the doubly excited systems of configurations. The singly excited system is built upon the parent terms, ^ML, in the $3d^5$ ground configuration of Mn III. Similarly, the doubly excited system is built upon the grandparent terms in the $3d^4$ ground configuration of Mn IV. The Mn II spectrum is predominantly comprised of transitions within the singly excited system, with the strongest being those between levels of the relatively well-known $3d^54s$ and $3d^54p$ configurations. This gives rise to a spectrum particularly rich in UV lines. Most of the levels of the singly excited system have previously been established, barring some of the higher-lying ($4d$, $5s$, $6d$...) levels. The levels of the doubly excited system,

$3d^4(^ML)nln'l'$, however, are incomplete and the transitions linking them to the singly excited system are weak.
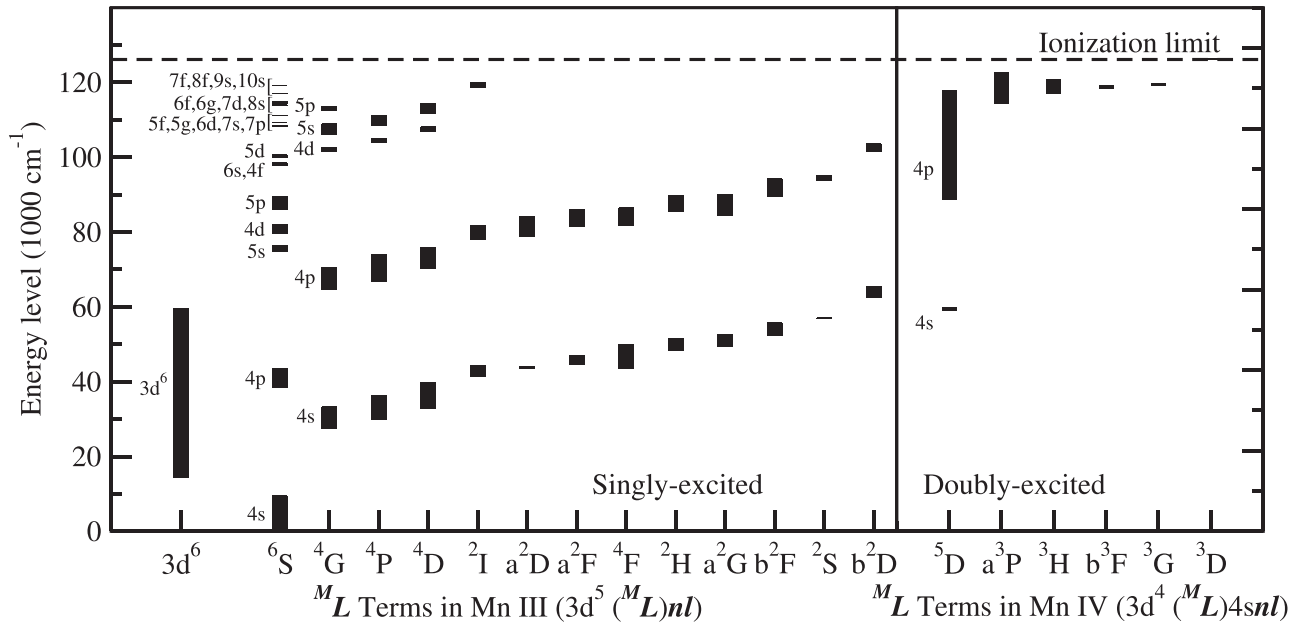
5. Level Optimization

Observed wavenumbers and uncertainties of transitions in Mn II were used in combination with the least-squares fitting program LOPT developed by Kramida (2011) at NIST, USA, to optimize the energy level values. The weighting assigned to each transition was given by the reciprocal of the square of the line's total estimated transition wavenumber uncertainty. Multiply identified lines were assigned a low weight within the fitting process so that the line parameters were retained but did not contribute to the level optimization. The optimization was done in several stages, starting with the strongest lines from a subset of the lowest even and odd energy levels measured in our FT spectra. The level values from this initial optimization were then used to improve the identification of lines in the observed spectrum. The optimization was then repeated several times, each time including weaker transitions and transitions to additional levels. At each stage of the optimization process, any lines that strongly deviated from the Ritz wavenumbers derived from the energy levels of that fit were checked for possible blends, misidentifications, or HFS. In these cases, the weighting was adjusted, the identification modified, or the wavenumber was remeasured by refitting the line. After as many as possible of the level values had been optimized using our FT spectra, the resulting level values were used to identify lines in the grating spectra. Lines in our grating spectra were necessary to optimize the values of the higher-lying levels and levels of the doubly excited system as these levels do not give strong lines in the wavelength region covered by our FT spectra. Finally, a search for transitions from new energy levels was made using the FT spectra.

All energy level values resulting from the analysis are presented in Table 5. This table includes the configuration, term, and J values of the energy level, optimized energy level value and its uncertainty, the difference between our new values and previous published values, and the number of lines used in the final level optimization.

5.1. Revision of Known Energy Level Values

A total of 505 of 532 energy level values from KS have been updated as a result of this analysis, and four term energies (for 12 levels) in KS have been resolved, giving 22 new energy level values. The differences, $E - E_{KS}$, between our 527 new energy level values and those of KS, are shown in Figure 3. Error bars represent the energy level uncertainties from both this analysis (black) and that of KS (red). With higher energy, there is a greater observed deviation from the mean. This can be attributed to the particularly large uncertainties given in previous measurements for the levels above $\approx 90,000\ cm^{-1}$. Many of the energy levels below this value are associated with the relatively well-known $4s$ and $4p$ configurations that have significantly smaller observed deviations and uncertainties.

Of the levels we were unable to update, the $z\ ^3K_8^\circ$ level given at $77,820.28\ cm^{-1}$ in KS has been discarded as it was determined by a single transition to a^3I_7 at $36,637.75\ cm^{-1}$. This line is doubly classified as $a\ ^3I_5 - z\ ^3K_6^\circ$, a transition that can account for all of the line's intensity. The remaining levels in KS are high excitation levels belonging to the $3d^5(^6S)7f$, $7g$, $8f$, $8g$, $8h$, and $9h$ configurations. These levels were previously

Figure 2. Term diagram showing the experimentally observed levels of of Mn II. The ionization limit of 126,145 cm^{-1} (Kramida 2011) is marked with a dashed line.
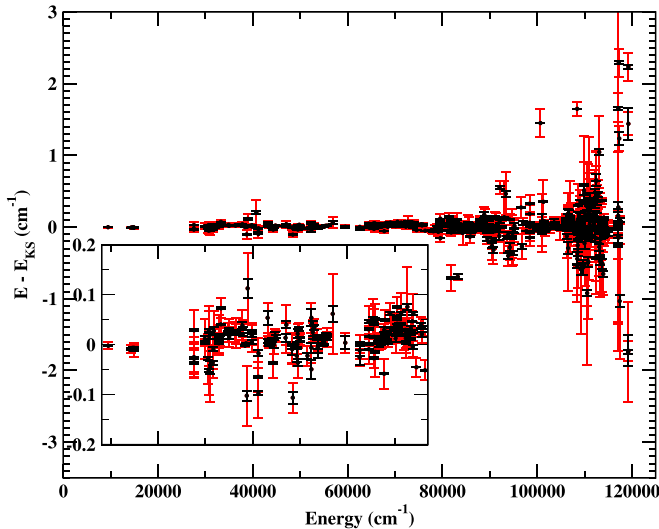
Figure 3. The difference, $E - E_{KS}$, between the optimized levels in this work and previously established energy level values of KS. Error bars: black, uncertainties from this work; red, uncertainties from KS. The inset shows the region from 8100 to 77,000 cm^{-1} on an expanded vertical scale.

Table 4
Changes in Mn II Energy Level Designations Compared with the Previous Compilation of KS

E^a (cm^{-1})	Previous Label (KS)	New Label
86,897.788	$(^5D)4s4p(^3P)\ w\ ^5P^\circ_3$	$(^6S)5p\ w\ ^5P^\circ_3$
86,936.921	$(^5D)4s4p(^3P)\ w\ ^5P^\circ_2$	$(^6S)5p\ w\ ^5P^\circ_2$
86,961.071	$(^5D)4s4p(^3P)\ w\ ^5P^\circ_1$	$(^6S)5p\ w\ ^5P^\circ_1$
88,840.07	$(^6S)5p\ v\ ^5P^\circ_1$	$(^5D)4s4p(^3P)\ v\ ^5P^\circ_1$
89,079.551	$(^6S)5p\ v\ ^5P^\circ_2$	$(^5D)4s4p(^3P)\ v\ ^5P^\circ_2$
89,429.390	$(^6S)5p\ v\ ^5P^\circ_3$	$(^5D)4s4p(^3P)\ v\ ^5P^\circ_3$
108,920.279	$w\ ^1H^\circ_5$	$(b^2G)4p\ w\ ^1H^\circ_5$
111,162.283	$s\ ^5P^\circ_1$	$(^6S)7p\ s\ ^5P^\circ_1$
111,178.700	$s\ ^5P^\circ_2$	$(^6S)7p\ s\ ^5P^\circ_2$
111,213.424	$s\ ^5P^\circ_3$	$(^6S)7p\ s\ ^5P^\circ_3$

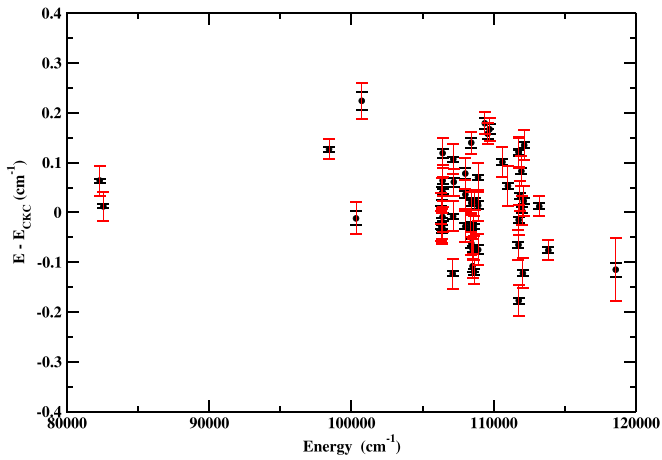**Note.**
[a] Energy level value from this work.

Table 4 gives a summary of the changes in level labels made, including the new and previous label used in KS for reference. Further details can be found in Liggins (2017).

5.2. Verification of Levels using FT Spectra

Since the last compilation of all known energy level values for Mn II by KS, a number of new energy level values have been identified by CKC using stellar spectral data. A total of 135 lines of the 278 Mn II lines classified by CKC were initially verified in our FT spectra. These were used to improve the energy level values of CKC and generate Ritz wavelengths that were used to identify additional lines in all our spectra. The wavenumbers and uncertainties of all the lines in our FT and grating spectra were then included into the level optimization.

Of the 73 new energy levels taken from CKC, 57 energy level values could be optimized using our FT spectra. The majority of these optimized levels belong to the $4d$ sub-configuration of the singly excited system with ^4G, ^4P, and ^4D

determined using visible and infrared transitions that are too weak to be seen in our FT spectra.

The lowest energy level uncertainties are from quintet and septet levels that have strong LS-allowed transitions to the ground level. These can be as low as ≈ 0.0015 cm^{-1} for the septet levels and ≈ 0.002–0.005 cm^{-1} for the quintet levels. The triplet and singlet levels do not have strong transitions to the ground level and hence the uncertainties of these levels are larger, ranging from 0.01 to 0.05 cm^{-1}. Levels that have been optimized solely using grating measurements may have uncertainties exceeding 0.1 cm^{-1} and include $3d^44s4p$ levels in the doubly excited system that only have transitions at shorter wavelengths than can be observed using our FT spectrometers.

Figure 4. The difference, $E - E_{CKC}$, between the optimized levels in this work and previously established energy level values of CKC. Error bars: black, uncertainties from this work; red uncertainties from CKC.

parent terms and have uncertainties between 0.002 and 0.005 cm^{-1}. Levels could not be verified if no transitions were observed to or from them (e.g., $(^2I)4d$ $^1K_7$), only one or two grating lines were seen (e.g., $(b^2D)4p$ $^3P_1^\circ$), or if the only lines observed were potentially blended (e.g., $(^6S)6f$ $^7F_{1,0}^\circ$). The levels $(^2I)4d$ $^1K_7$ at 119,152.797 cm^{-1} and $(^4P)4d$ $^3F_2$ at 110,664.62 cm^{-1} could not be verified, as all of the lines in CKC involving these levels either did not appear in our spectra or were classified using other transitions. A new value for the $(^2I)4d$ $^1K_7$ level was found at 119,184.742 cm^{-1}, based on three lines in our FT spectra and two lines in our grating spectra. The value of the $(^4P)4d$ $^3F_2$ level was changed to 110,640.031 cm^{-1}, based on one line in our FT spectra and nine lines in our grating spectra.

The differences, $E - E_{CKC}$, between our updated energy level values and those of CKC, are shown in Figure 4. Error bars represent the energy level uncertainties derived from this work (black), and those as estimated for the levels given by CKC (red). Since no level uncertainties were given by CKC, an estimate was derived from their wavelength uncertainty. This was then combined with an averaged uncertainty in the lower levels from KS that are linked to the upper level. These estimates range from ≈0.02 to 0.06 cm^{-1}.

Our new values and uncertainties for these 59 levels are included in Table 5 and are marked with "C" in the last column.

5.3. New Energy Levels

After revision of known energy levels, the line list from our FT and grating spectra was used to search for new energy levels. The theoretical calculations of Kurucz (2016) predicting level energies and line transition probabilities were a very helpful aid in searching for new levels. The unpublished list of 53 energy levels by Joueizadeh et al. (1995) was available without any details of analysis or corresponding transitions. Among these levels, 25 were confirmed by the determination of CKC. The remaining 28 levels served as an initial guide for the present analysis. They are now firmly established as new energy levels by a large number of classified transitions in our new spectra, and their energy values are optimized using the present high-precision measurements. In addition, 22 new level

energies were found to replace the previous four unresolved energies reported in KS for the ^7G and ^5G terms of the $(^6S)5g$ and $6g$ subconfigurations. All new levels belong to the $(^6S)6d$, $5g$, $6g$, $(^4G)4d$, $(^4P)4d$ and $(^4D)4d$ subconfigurations.

5.3.1. New Levels of the $3d^5(^6S)6d$ ^5D Term

The five levels of the $(^6S)6d$ ^5D term are predicted by the calculations of Kurucz (2016) to have significant mixing with levels of the $(^4D)4d$ ^5D and $(^4P)4d$ ^5D terms. This gives rise to strong observed transitions from these $6d$ levels to the $(^4D)4p$ and $(^4P)4p$ subconfigurations, with the strongest observed transitions from the $(^6S)6d$ ^5D levels being to levels of the $(^4D)4p$ x $^5P^\circ$ term. A total of 68 newly classified lines have been identified as transitions from levels of the $(^6S)6d$ ^5D term, of which 38 are from our FT spectra. The uncertainties in energy values resulting from the level optimization are as low as 0.0024 cm^{-1}, for $J = 4$, up to 0.008 cm^{-1} calculated for the $J = 0$ level, from which only one weak line was observed in our FT spectra, and only two lines in our grating spectra.

5.3.2. New Levels of the $(^4G)4d$ Subconfiguration

Four new levels in the $(^4G)4d$ configuration have been established for the ^5D term. Kurucz (2016) has calculated a degree of mixing in the level compositions (with those of the $(^6S)6d$ ^5D and $(^6S)5d$ ^5D terms), but with the $(^4G)4d$ ^5D term contributing at least 65% of the level compositions, most of the transitions from these levels are those that would be expected without mixing. Each level gives at least one spectral line in our FT spectra and several in our grating spectra. The calculated uncertainties in the energy level values are between 0.003 and 0.006 cm^{-1}. A total of 67 Mn II lines have been newly classified using these level values, of which 16 are from our FT spectra.

5.3.3. New Levels of the $(^4P)4d$ Subconfiguration

New level values have been obtained for the $(^4P)4d$ ^5D term ($J = 0...4$) using strong lines to levels of the $(^4P)4p$ and $(^4D)4p$ subconfigurations present in our FT spectra. A total of 70 lines have been newly classified from these level values, of which 22 are in our FT spectra. The resulting $(^4P)4d$ ^5D energy level values have been given with uncertainties of 0.003–0.007 cm^{-1}.

New energy values have been found for the $(^4P)4d$ $^3P_1$ and $(^4P)4d$ $^3P_0$ levels. These new levels complete the ^3P term, following our verification of the $^3P_2$ level found by CKC. This term contributes 11 lines in our FT spectra and 25 lines in our grating spectra. Our new value for the $(^4P)4d$ $^3F_4$ level completes the ^3F term, classifying eight lines in our FT spectra and five lines in our grating spectra.

5.3.4. New Levels of the $(^4D)4d$ Subconfiguration

New energy values for 11 levels in the $(^4D)4d$ configuration have been found as part of this analysis with level uncertainties between 0.002 and 0.009 cm^{-1}.

Energy values for the $(^4D)4d$ $^5P_1$ and $(^4D)4d$ $^5P_2$ levels were fitted using 26 lines, 11 of which were measured using FT spectroscopy. These new levels complete the ^5P term for this subconfiguration, with the level $^5P_3$, found by CKC, verified with both our FT and grating spectra. A new value has been found for the $^5F_1$ level, completing the ^5F term for the $(^4D)4d$

Table 5
Energy Levels of Mn II

Energy Level			E (cm^{-1})	Unc. (cm^{-1})	$E - E_{\mathrm{old}}$ (cm^{-1})	Flag	No. of Lines
Configuration	Term	J					
$3d^5(^6S)4s$	$a\ ^7S$	3	0.0000	0.0000	0.000		51
$3d^5(^6S)4s$	$a\ ^5S$	2	9472.9913	0.0009	-0.002		64
$3d^6$	$a\ ^5D$	4	14,325.8547	0.0010	-0.011		84
$3d^6$	$a\ ^5D$	3	14,593.8286	0.0010	-0.006		96
$3d^6$	$a\ ^5D$	2	14,781.1974	0.0010	-0.008		87
$3d^6$	$a\ ^5D$	1	14,901.1979	0.0010	-0.005		63
$3d^6$	$a\ ^5D$	0	14,959.8668	0.0011	-0.009		25
$3d^5(^4G)4s$	$a\ ^5G$	6	27,547.2300	0.0020	-0.030		34
$3d^5(^4G)4s$	$a\ ^5G$	5	27,571.2081	0.0019	-0.042		57
$3d^5(^4G)4s$	$a\ ^5G$	4	27,583.5643	0.0018	-0.026		65
$3d^5(^4G)4s$	$a\ ^5G$	3	27,588.5046	0.0016	-0.025		65
$3d^5(^4G)4s$	$a\ ^5G$	2	27,589.3904	0.0019	0.030		44
…							
$3d^5(^4G)4d$	^5F	5	106,298.933	0.006	-0.027	C,J	9
$3d^5(^4G)4d$	^5F	4	106,324.766	0.005	0.008	C,J	12
$3d^5(^4G)4d$	^5F	3	106,340.452	0.008	-0.033	C,J	12
$3d^5(^4G)4d$	^5F	2	106,348.432	0.011	-0.022	C	10
$3d^5(^4G)4d$	^5F	1	106,351.620	0.013	0.038	C	7
$3d^5(^4G)4d$	^5G	6	106,387.279	0.005	-0.031	C,J	5
$3d^5(^4G)4d$	^5G	5	106,400.757	0.008	-0.009	C,J	8
$3d^5(^4G)4d$	^5G	4	106,406.683	0.005	0.041	C,J	9
$3d^5(^4G)4d$	^5G	2	106,408.075	0.006	0.064	C	5
$3d^5(^4G)4d$	^5G	3	106,408.467	0.009	0.119	C	11

Note. Columns 1, 2, and 3 give the electronic configuration, spectroscopic term, and J value respectively. The energy level value, E, from this work is given in column 4 and is rounded according to its uncertainty in column 5. The uncertainty is given relative to ground, rounded so that the uncertainty in units of the last digit does not exceed 25. $E - E_{\mathrm{old}}$ is the difference between our energy values and previous values, E_{old}. Flag: C—previous value from CKC; J—previous value from Joueizadeh et al. (1995) if not in CKC; R—new energy level value replaces previously published unresolved single value for all levels of the term in KS; No flag—previous value from KS. "No. of lines" gives the number of significant transitions used in fitting the energy level value, omitting lines that are the sole transition to another energy level.

(This table is available in its entirety in machine-readable form.)

configuration, following the verification of the CKC $J = 5, 4, 3, 2$ levels.

The $^3S_1$ level has been found using three weak lines in our FT spectra to the $(^4D)4p\ y\ ^3P°$ and $(^4P)4p\ z\ ^3P°$ terms and verified using four lines in our grating spectra. New levels for $J = 3, 2, 1$ of the $(^4D)4d\ ^5D$ term have been found using 29 lines in our FT spectra and 37 lines in our grating spectra, with the $J = 4$ level previously established by CKC. The remaining $J = 0$ level has yet to be found. The uncertainties of these levels are as low as $\approx 0.002\ \mathrm{cm}^{-1}$.

Levels $^3F_3$ and $^3F_2$ of the $(^4D)4d$ configuration have been found using seven lines in our FT spectra to levels of the $(^4D)4p\ y\ ^3D°$ and $(^4D)4p\ y\ ^3F°$ terms and verified with an additional 15 lines in our grating spectra. No levels had previously been established for the ^3F term, and the level for $J = 4$ is still missing.

Finally, new energy values have been found for the levels $^3D_3$ and $^3D_2$ using transitions to the $(^4D)4p\ y\ ^3P°$ term in our FT spectra, with the predicted level $^3D_1$ still missing. Our FT spectra also show transitions to the $(^4D)4p\ y\ ^3D°$ term from $(^4D)4d\ ^3D_2$. In total, 18 transitions have been identified using 6 observed lines in our FT spectra and 12 lines in our grating spectra. Although the $^3D_3$ level gives only a single line in our FT spectra and three lines in our grating spectra, the classifications of the lines are justified by their consistency with those for the level $^3D_2$.

5.3.5. New Levels of the $(^6S)5g$ and $(^6S)6g$ Subconfigurations

Previously, KS had assigned just one energy value for the ^7G terms of the $(^6S)5g$ and $(^6S)6g$ subconfigurations. For the ^5G terms, KS had assigned the same energy value for each of the five levels of the terms. Lines due to transitions involving these levels have been resolved in our FT spectra, allowing new energy values to be assigned to 12 levels to replace the previous two approximate values of KS, for $(^6S)5g\ ^7G$ with $J = 1, 2, 3, 4, 5, 6, 7$ and $(^6S)6g\ ^7G$ with $J = 3, 4, 5, 6, 7$, and new energy values assigned to a further 10 levels to replace two approximate values of KS for $(^6S)5g\ ^5G$ with $J = 1, 2, 3, 4, 5$ and $(^6S)6g\ ^5G$ with $J = 1, 2, 3, 4, 5$. Thirty-seven lines have been classified from these levels in our FT spectra. Uncertainties for the majority of the new levels are better than $0.006\ \mathrm{cm}^{-1}$.
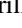
6. Conclusions

Accurate atomic data for Mn II are needed in the analysis of astrophysical spectra, particularly in the study of sharp-lined, chemically peculiar stars for which there is an observed overabundance of manganese. The last compilation of wavelengths and energy levels for Mn II is predominantly based on measurements that predate the development of high-resolution FT spectroscopy and are of insufficient accuracy for modern astrophysical analyses.

A large-scale analysis of the FT spectrum of Mn II, in the range 1820–58,990 cm^{-1}, has enabled the classification of 1364 transitions, with wavenumbers found to typically at least an order of magnitude lower uncertainty compared with those of previous measurements. New supplementary grating spectra, covering the wavenumber region 28,385–121,728 cm^{-1}, extended this analysis, allowing the classification of 4892 additional transitions of Mn II, with wavelength uncertainties between 0.0002 and 0.0005 nm.

This extensive term analysis has resulted in the optimization of 505 of the previously reported energy level values of KS; has allowed 57 energy level values, previously derived from stellar spectra by CKC, to be verified with laboratory FT spectroscopy; and has enabled the identification of 52 new energy levels in Mn II, from which 430 lines have been newly classified. In total, new accurate data are presented for 614 Mn II energy levels and 6019 lines. We anticipate that our new measurements will allow a more reliable analysis of Mn II spectral lines in astrophysical spectra.

ORCID iDs

Florence S. Liggins ⓘ https://orcid.org/0000-0003-3448-4704
Juliet C. Pickering ⓘ https://orcid.org/0000-0003-2879-4140
Gillian Nave ⓘ https://orcid.org/0000-0002-1718-9650
Jacob W. Ward ⓘ https://orcid.org/0000-0002-5841-0649
W.-Ü L. Tchang-Brillet ⓘ https://orcid.org/0000-0001-9790-9947

References

Blackwell-Whitehead, R. J. 2003, PhD thesis, Imperial College, Univ. of London
Blackwell-Whitehead, R. J., Pickering, J. C., Pearse, O., & Nave, G. 2005, ApJS, 157, 402
Carpenter, K. G., Ayres, T. R. & the ASTRAL Science Teams 2015, in 18th Cambridge Workshop on Cool Stars, Stellar Systems, and the Sun, ed. G. T. van Belle & H. C. Harris, 1041
Castelli, F., Kurucz, R. L., & Cowley, C. R. 2015, A&A, 580, A10
Catalán, M. A. 1923, RSPTA, 233, 127
Clear, C. P. 2018, PhD thesis, Imperial College London, doi:10.25560/75141
Curtis, C. W. 1938, PhRv, 53, 474
Curtis, C. W. 1952, JOSA, 42, 300
Danzmann, K., Günther, M., Fischer, J., Kock, M., & Kühne, M. 1988, ApOpt, 27, 4947
Davis, S. P., Abrams, M. C., & Brault, J. W. 2001, Fourier Transform Spectrometry (New York: Academic)

García-Riquelme, O., Iglesias, L., & Velasco, R. 1957, Anales Real Soc. Espan. Fis. Quim., 53-A, 77
Griesmann, U., Kling, R., Burnett, J. H., Bratasz, L., & Gietzen, R. A. 1999, Proc. SPIE, 3818, 180
Holmes, C. E. 2015, PhD thesis, Imperial College London, doi:10.25560/34943
Holt, R. A., Scholl, T. J., & Rosner, S. D. 1999, MNRAS, 306, 107
Iglesias, L. 1956, JOSA, 46, 449
Iglesias, L. 1957, JOSA, 47, 852
Iglesias, L., & Velasco, R. 1963, Anales de Fisica y Quimica, 54 (A), 227
Iglesias, L., & Velasco, R. 1964, Publ. Inst. Opt. Madrid, 23, 1
Johansson, S., Wallerstein, G., Gilroy, K. K., & Joueizadeh, A. 1995, A&A, 300, 521
Joueizadeh, A., Litzén, U., Johansson, S., et al. 1995, in 5th Int. Coll. on Atomic Spectra and Oscillator Strengths for Astrophysical and Laboratory Plasmas, Poster Papers, ed. W.-Ü. L. Tchang-Brillet, J.-F. Wyart, & C. Zeippen (Meudon: Publications de l'Observatoire de Paris)
Kling, K., & Griesmann, U. 2000, ApJ, 531, 1173
Kramida, A., Nave, G., & Reader, J. 2017, Atoms, 5, 9
Kramida, A., Ralchenko, Yu., Reader, J. & NIST ASD Team 2019, NIST Atomic Spectra Database (v5.7.1), https://physics.nist.gov/asd
Kramida, A., & Sansonetti, J. E. 2013, ApJS, 205, 14
Kramida, A. E. 2011, CoPhC, 182, 4419
Kramida, A. E., & Nave, G. 2006, EPJD, 39, 331
Kurucz, R. L. 2011, CaJPh, 89, 417
Kurucz, R. L. 2016, Atomic Data, http://kurucz.harvard.edu/atoms/2501/
Learner, R. C. M., & Thorne, A. P. 1988, JOSAB, 5, 2045
Liggins, F. S. 2017, PhD thesis, Imperial College London, doi:10.25560/59134
Litzén, U., Brault, J. W., & Thorne, A. P. 1993, PhyS, 47, 628
Makaganiuk, V., Kochukhov, O., Piskunov, N., et al. 2012, A&A, 539, A142
Mashonkina, L. 2010, in EAS Publications Series 43, Non-LTE Line Formation for Trace Elements in Stellar Atmospheres, ed. R. Monier et al. (Les Ulis: EDP Sciences), 215
Mashonkina, L. 2013, in Proc. IAU Symp. 298, Setting the Scene for Gaia and LAMOST, ed. S Feltzing et al. (Cambridge: Cambridge Univ. Press), 355
Nave, G., Griesmann, U., Brault, J. W., & Abrams, M. C. 2015, Xgremlin: Interferograms and spectra from Fourier transform spectrometers analysis, Astrophysics Source Code Library, ascl:1511.004
Nave, G., Li, Z., Sansonetti, C. J., Griesmann, U., & Fried, A. D. 2005, PhST, T119, 35
Nave, G., Sansonetti, C. J., Townley-Smith, K., et al. 2017, CaJPh, 95, 811
Peck, E. R., & Reeder, K. J. 1972, JOSA, 62, 958
Pulliam, B. V. 1979, MS thesis, Purdue Univ.
Racah, G., & Shadmi, Y. 1959, Bull. Res. Counc. Israel F, 8, 15
Racah, G., & Spector, N. 1960, Bull: Math. Phys., 9, 75
Saffe, C., Nunez, N., & Levato, H. 2011, RMxAA, 47, 219
Saloman, E. B., & Sansonetti, C. J. 2004, JPCRD, 33, 1113
Sansonetti, J. E., Reader, J., Sansonetti, C. J., & Acquista, N. 1992, J. Res. Natl. Inst. Stand. Technol., 97, 1
Schöller, M., Hubrig, S., Correia, S., Ilyin, I., & Gonzalez, J. F. 2013, CEAB, 37, 369
Sigut, T. A. A. 2001, A&A, 377, L27
Tchang-Brillet, W.-Ü. L., & Azarov, V. I. 2002, PhST, T100, 104
Thorne, A. 1996, PhST, T65, 31
Thorne, A. P., Harris, C. J., Wynne-Jones, I., Learner, R. C. M., & Cox, G. 1987, JPhE, 20, 54
Tomkins, F. S., & Fred, M. 1951, JOSA, 41, 641
Townley-Smith, K., Nave, G., Pickering, J. C., & Blackwell-Whitehead, R. J. 2016, MNRAS, 461, 73
Whaling, W., Anderson, W. H. C., Carle, M. T., Brault, J. W., & Zarem, H. A. 1995, JQSRT, 53, 1
Whaling, W., Anderson, W. H. C., Carle, M. T., Brault, J. W., & Zarem, H. A. 2002, J. Res. Natl Inst. Stand. Technol., 107, 149